Statics Optimization of a Hexapedal Robot Modelled as a Stewart Platform

Enrico Donato[1], Giacomo Picardi[1] and Marcello Calisti[2]

[1] The Biorobotics Institute, Sant'Anna School of Advanced Studies, Pisa, Italy
[2] Lincoln Institute for Agri-food Technology, University of Lincoln, Lincoln, UK

Abstract. SILVER2 is an underwater legged robot designed with the aim of collecting litter on the seabed and sample the sediment to assess the presence of micro-plastics. Besides the original application, SILVER2 can also be a valuable tool for all underwater operations which require to interact with objects directly on the seabed. The advancement presented in this paper is to model SILVER2 as a Gough-Stewart platform, and therefore to enhance its ability to interact with the environment. Since the robot is equipped with six segmented legs with three actuated joints, it is able to make arbitrary movements in the six degrees of freedom. The robot's performance has been analysed from both kinematics and statics points of view. The goal of this work is providing a strategy to harness the redundancy of SILVER2 by finding the optimal posture to maximize forces/torques that it can resist along/around constrained directions. Simulation results have been reported to show the advantages of the proposed method.

Keywords: Legged Robot · Parallel Robot · Statics · Manipulability

1 Introduction

Mobile robots, with their ability of moving in space, represent the possibility of extending the work-space of robotics and opened the way to explorations and interventions in areas which are normally inaccessible to humans [1]. Besides the more established categories such as wheeled robots [2], aerial drones [3], underwater vehicles [4], several mobile bio-inspired robots have been recently presented [5] with the promise of augmented exploration capabilities. Legged robotics is probably the most studied category of bio-inspired mobile robots due to their potential of adapting to irregular terrains, negotiate obstacles and interact gently with surroundings [6].

When a mobile robot is equipped with a manipulator we speak of mobile manipulation. This allows to harness the locomotion ability of mobile robots to extend the work-space of the manipulator and perform manipulation tasks in previously inaccessible locations. Depending on the category of mobile robot on which the manipulator is mounted on, different challenges arise [7]. On ground-based mobile manipulation, either implemented on wheeled/tracked [8] or legged vehicle [9,10], the mobile robot is capable of providing sufficient reaction force at the base of the manipulator while holding its position. Moreover, the redundancy provided by multiple articulated legs allows to implement different strategies for

manipulation: on one hand the same linkage can be used for both locomotion and manipulation, as presented in [11], and on the other when the robot is in a fixed position, legs can be used to change the position and orientation of the base of the manipulator as proposed in [12,13].

In the underwater environment, robots are used for a wide set of manipulation tasks which range from opening and closing valves to collecting biological samples. Despite its inherent complexity, the field of floating manipulation has made remarkable progresses and the development of propeller-driven autonomous intervention robots (Intervention AUV, or I-AUV) is currently among the most interesting research topics in robotics [14]. However, some intrinsic limitations still exists such as raising debris with the perturbation introduced by the thrusters, introducing significant acoustic noise, and counteracting high forces at the manipulator without the reaction force provided by the ground. For this reason, the novel category of underwater legged robots, of which SILVER2 [14] is one representative, may be an effective solution to manipulation tasks when operations are carried out directly on the seabed. In a previous work [15] SILVER2 demonstrated the ability to collect different objects using a soft manipulator and its maximum lifting force was experimentally assessed.

To improve adaptability to different tasks and environments, Reconfigurable Parallel Platform (RPP) [16,17] are gaining more attention, such as Free-Hex [18]. SILVER2 is an hexapedal robot with 3-dofs legs, and could be considered a RPP since it has not a base anchored to the ground, but movable. The articulated legs improve the workspace with respect to its linear counterpart [19].

In this work, we modelled SILVER2 as a Gough-Stewart (GS) platform, a classic parallel robot consisting of a platform actuated by six linear pistons. This allowed us to solve the inverse kinematic problem and compute the joint angles to set a desired position and attitude of SILVER2 body. The performance obtained in [20] could be further improved by distributing the forces more efficiently and adapting the positioning of the legs to specific manipulation task. On top of this, following the results presented in [21], we derived the manipulability ellipsoids of SILVER2 and set up an optimization problem to find the legs configuration which maximizes the forces/torques that the robot can resist along a preferred direction. Since the derivations presented in this work pertain to the statics of the robots, hydrodynamic contributions do not hold and the results obtained are valid also for terrestrial hexapedal robots.

2 Materials and Methods

SILVER2 is modeled as a parallel manipulator and its Inverse Kinematics (IK) and Differential Kinematics (DK) are presented. Force ellipsoids are introduced to compute its Statics, and an optimization algorithm is set to find the legs configuration which maximizes forces and torques along/around arbitrary axes.

Symbol	*Format*	*Description*
t	$\Re^{3\times1}$	Translation of the body from the ground
R_{xy}	$\Re^{3\times3}$	Rotation matrix of {y} wrt {x}
ω_x	$\Re^{3\times1}$	Angular velocities of the body in {x}
l_x	$\Re^{3\times1}$	Feet position wrt {x}.
q_i	$\Re^{3\times1}$	i-th leg joints angles
$J_l(q_i)$	$\Re^{3\times3}$	i-th leg Jacobian matrix
J_{P_T}, J_{R_T}	$\Re^{18\times3}$	Linear/Angular SILVER2 Jacobian matrix
v_i	$\Re^{3\times1}$	i-th ellipsoid's axis vector
λ_i	$\Re$	i-th ellipsoid's semi-axis length

Table 1: Summary of most common used symbols. Subscripts omitted when considered wrt world reference frame.

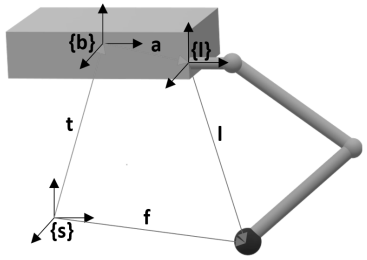

Fig. 1: Inverse Kinematics of the Stewart platform adapted to SILVER2

2.1 Kinematics of the GS platform

To solve the IK of the platform, we take into account the world $\{s\}$, the robot's body $\{b\}$ and the legs base $\{l\}$ reference frames. We choose $R_{sb} = R_{sl}$. By taking as a reference Fig.1, the feet position in the leg reference frames is:

$$l_l = R_{bs}(f - t) - a_b \tag{1}$$

The length of the leg is the vector norm of Eq.(1): $\|l_l\| = \sqrt{l_l^T l_l}$.

In the case of the Gough-Stewart platform, the DK has already been analysed [22], and it accounts just for six linear actuators. By extension to our case, both members of Eq.(1) can be multiplied by R_{sb}. For the i-th leg:

$$R_{sb}l_{l,i} = f_i - t - R_{sb}a_b \tag{2}$$

By differentiation with respect to time:

$$[\omega]R_{sb}l_{l,i} + R_{sb}\dot{l}_{l,i} = \dot{f}_i - \dot{t} - [\omega]R_{sb}a_b - R_{sb}\dot{a}_b \tag{3}$$

where $[\omega]$ is the skew-symmetric matrix of of the angular velocity ω, and the notation $\dot{x}$ is the time derivative of x. The linear velocity of the feet on $\{s\}$ is null $\dot{f}_i = 0$, since they are supposed to be fixed. Moreover, the distance of the leg anchor point to the center of geometry of the body will not change, since the body is rigid, thus $\dot{a}_b = 0$. Consequently, the Eq.(3) can be simplified to

$$\dot{l}_{l,i} = -(R_{bs}\dot{t} + R_{bs}[\omega]R_{sb}(a_b + l_{l,i})) = -(\dot{t}_b + [\omega_b](a_b + l_{l,i})) \tag{4}$$

Eq.(4) strictly relates the moving platform to the leg in the velocity space: both linear and angular speed of the body are affected by the leg change-over.

2.2 Kinematics adapted to SILVER2

SILVER2 has six segmented legs instead of linear actuators: to inherit the IK solution of the GS platform [23], the length vectors of the linear legs of the GS platform are used as input to the IK of the SILVER2's segmented legs. When SILVER2 contacts the ground with all legs, it creates 5 closed chains (by pairing two consecutive legs together); then, they generate $5 \times 6 = 30$ constraints. The tip of the leg is able to omnidirectionally rotate on the ground, thus we consider it as a passive spherical joint. Each leg has 6 DoFs (three of them come from the actuated joints, while the others from the spherical joint), with a total of $6 \times 6 = 36$ DoFs. Consequently, there will be $36 - 30 = 6$ independent DoFs, that coincide with position and orientation of the robot's body.

The velocity of the feet with respect to the leg anchor point comes from the discussion of its DK; indeed, it is a function of the joint angular velocities, that can be substituted in Eq.(4).

$$J_l(q_i)\dot{q}_i = -(\dot{t}_b + [\omega_b](a_b + l_{l,i})) \tag{5}$$

where $J_l(q_i)$ is the analytical Jacobian of the i-th leg and q_i is the respective joint angles vector. $J_l(q_i)$ is assumed to be invertible, and it happens whenever the legs are not in a singular configuration (the IK of the leg always admits only one solution because of mechanical constraints [24]). Moreover, the cross-product property of the skew-symmetric matrix is exploited.

$$\dot{q}_i = -J_l^{-1}(q_i)\dot{t}_b - J_l^{-1}(q_i)[\omega_b](a_b + l_{l,i}) \tag{6}$$

Considering a generic matrix $A \in \Re^{3\times3}$ and two vectors $b, c \in \Re^{3\times1}$, it holds that $A(b \times c) = -(A^T \times c)^T b$. The cross product between A and c is a matrix whose columns are the cross product between the respective column of A and c. Therefore, Eq.(6) can be simplified to

$$\begin{gathered} \dot{q}_i = -J_l^{-1}(q_i)\dot{t}_b + (J_l^{-T}(q_i) \times (a_b + l_{l,i}))^T \omega_b = J_{P_i}^{-1} \begin{bmatrix} \dot{t}_b \\ \omega_b \end{bmatrix} \\ J_{P_i}^{-1} = [-J_l^{-1}(q_i), (J_l^{-T}(q_i) \times (a_b + l_{l,i}))^T] \end{gathered} \tag{7}$$

Starting from the inverse kinematics of the Stewart Platform, the inverse Jacobian $J_{P_i}^{-1} \in \Re^{3\times6}$ has been computed. $J_{P_i}^{-1}$ is the contribute of the i-th leg to the parallel robot's inverse Jacobian. In the case that only linear velocities are considered ($\omega = 0$), the forward Jacobian can be obtained via the Jacobian matrix pseudo-inverse:

$$\begin{bmatrix} \dot{q}_1 \\ \vdots \\ \dot{q}_6 \end{bmatrix} = \begin{bmatrix} -J_L^{-1}(q_1) \\ \vdots \\ -J_L^{-1}(q_6) \end{bmatrix} \dot{\bar{t}} \quad \rightarrow \quad \dot{Q} = J_{P_T}^{-1}(Q)\dot{t} \tag{8}$$

$$J_{P_T}(Q)\dot{Q} = \dot{t}, \quad J_{P_T}(Q) = (J_{P_T}^{-T}(Q)J_{P_T}^{-1}(Q))^{-1}J_{P_T}^{-T}(Q) \tag{9}$$

The same procedure can be applied in the case $\dot{t} = 0$, when only angular velocities are considered.

$$J_{P_R}(Q)\dot{Q} = \omega \tag{10}$$

The kinematic features of the hexapod are necessary to assess its statics. In particular, the manipulability of SILVER2 will be exploited in the next sections.

2.3 Manipulability of Parallel Manipulators

At a kinematic singularity, a robot's end-effector loses the ability to translate or rotate in one or more directions. The manipulability ellipsoid $E_M = (JJ^T)^{-1}$ allows one to geometrically visualize the directions in which the end-effector moves with least or greatest effort. It corresponds to the end-effector velocities for joint rates $\dot{q}$ satisfying $||\dot{q}|| = 1$. Like for manipulability ellipsoids, the force ellipsoid $E_F = JJ^T$ can be found for joint torques τ satisfying $||\tau|| = 1$. It holds that $E_F E_M = I$, so the two ellipsoids are orthogonal and their product is a unit sphere in the three-dimensional space.

The equivalent to manipulability and force ellipsoids can be constructed even with respect to angular velocities and torques, by taking as a reference the Jacobian matrix of the parallel robot related to angular motions expressed in Eq.(10).

If the ellipsoid is not rotated with respect to the frame axes, it is represented by the quadratic curve

$$\frac{x^2}{\rho_1^2} + \frac{y^2}{\rho_2^2} + \frac{z^2}{\rho_3^2} = 1 \tag{11}$$

where ρ_i is the length of the i-th semi-axis. An ellipsoid is uniquely defined by its axes of symmetry v_i and the length of respective semi-axes ρ_i, which correspond to the eigenvectors and eigenvalues of the matrix $E \in \Re^{3\times3}$. A custom ellipsoid is computed via the Eq.(12), where $v_i \cdot v_j = 0, i \neq j$.

$$E = \begin{bmatrix} | & | & | \\ v_1 & v_2 & v_3 \\ | & | & | \end{bmatrix} \begin{bmatrix} \|\lambda_1\| & 0 & 0 \\ 0 & \|\lambda_2\| & 0 \\ 0 & 0 & \|\lambda_3\| \end{bmatrix} \begin{bmatrix} | & | & | \\ v_1 & v_2 & v_3 \\ | & | & | \end{bmatrix}^{-1} \tag{12}$$

From Eqs.(11)-(12) it holds that the length of the manipulability ellipsoid's i-th semi-axis is $\rho_i = 1/\sqrt{\|\lambda_i\|}$, where λ_i is the i-th eigenvalue. The greater ρ_i is, the more easily the end-effector can move in the v_i direction. The force ellipsoid is obtained from the manipulability ellipsoid simply by stretching it along v_i by a factor $1/\|\lambda_i\|$.

In order to define how close the robot is to a singular configuration, we resorted to condition number μ [25], defined as the ratio between the highest and the lowest eigenvalues of E. If $\mu = 1$, the ellipsoid is spherical and the end-effector is able to move towards any direction with the same ability; when the robot approaches a singularity, then $\mu \to +\infty$.

$$\mu = \frac{\lambda_{\max}}{\lambda_{\min}} \geq 1 \tag{13}$$

Another common measure is the *manipulability index* [26], that is proportional to the volume of the ellipsoid. If the structure tends to a singularity, then $MI \to 0$.

$$MI = \sqrt{\| \det JJ^T \|} = \sqrt{\|\lambda_1 \lambda_2 \lambda_3\|} \geq 0 \tag{14}$$

2.4 Statics optimization

Manipulation tasks with SILVER2 may require high forces along certain axes. Exploiting force ellipsoids, the longest semi-axis should be parallel to the direction in which the highest force needs to be exerted. The same concept can be applied to the rotational case: the axis of symmetry should be parallel to the direction around which the highest torque has to be applied. By keeping the body in a fixed pose, the goal is to identify a new admissible legs configuration that achieves the aforementioned objectives.

A non-linear optimization problem is constructed. The optimization variables $q_i, i = 1, \cdots, 18$ coincide with the leg joint angles. The position of feet and knees with respect to the anchorage points of the legs are identified via their forward kinematics. In addition, the force ellipsoid of the parallel robot can be constructed as previously discussed.

The objective function exploits the largest projection of the force ellipsoid's axes along a given direction $\bar{G} \in \Re^{3\times 1}$. Consequently, the optimal solution coincides with the legs configuration which maximize the projection of the force ellipsoid along $\bar{G}$.

$$\max_{\boldsymbol{q}} \max_{i} \left[\frac{v_i}{\sqrt{\lambda_i}} \cdot \bar{G} \right], i = 1, 2, 3 \tag{15}$$

The admissibility of a solution is assessed by satisfying the following constraints [$i \in \{1, 2, 3\}$, $j \in \{1, \cdots, 6\}$].

(a) *Joints* can rotate in limited ranges.

$$q_{\min,i} \leq q_i \leq q_{\max,i} \tag{16}$$

(b) *Feet* have to lie at zero height and the central legs has to be positioned among the lateral ones in the y-direction.

$$l_{z,j} = 0 \qquad l_{y,3} \leq l_{y,2} \leq l_{y,1} \qquad l_{y,6} \leq l_{y,5} \leq l_{y,4} \tag{17}$$

Moreover, central legs' feet will never be under the body for stability reasons.

$$l_{x,2} \geq \text{body\_width}/2 \qquad l_{x,5} \leq -\text{body\_width}/2 \tag{18}$$

(c) Constraints on *knees* are similar to those on feet. The height of the knee must always be greater than zero, since the legs cannot penetrate the ground.

$$k_{z,j} \geq 0 \qquad k_{y,3} \leq k_{y,2} \leq k_{y,1} \qquad k_{y,6} \leq k_{y,5} \leq k_{y,4} \tag{19}$$

The algorithm needs an initial guess to find the optimal solution: since the initial pose of the body is fixed and known, the IK of the hexapod is computed and used as starting solution. The optimal solution is an admissible configuration of SILVER2, and its force ellipsoid has the highest projection along the given direction with respect to other admissible configurations. In any case, the robot will tend to take on a configuration closer and closer to one of its singularities.

3 Results

Results come from simulations, which find and show the optimal solutions to the respective problems. The optimizer is based on the *fmincon* function with the *sqp* algorithm, from the Matlab Optimization Toolbox; it looks for the minimum of a constrained nonlinear multivariable function. Bounds to variables and non-linear inequalities have been considered.

The optimization strategy of the SILVER2 Statics is tested against chosen directions, which coincide with the standard basis of the three-dimensional space.

$$\bar{G}_x = [1,0,0]^T \qquad \bar{G}_y = [0,1,0]^T \qquad \bar{G}_z = [0,0,1]^T \tag{20}$$

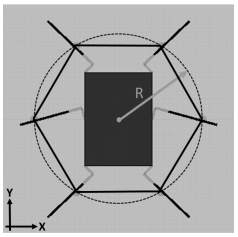

Fig. 2: Leg tips are placed on the vertexes of the regular hexagon. The choice of r affects the initial guess of the problem.

The initial guess of the optimization problem is chosen by arbitrarily setting the side length r of the regular hexagon on whose vertexes the feet are placed, and the quote of the body. The body and the ground are considered to be coplanar in the following simulations. The optimization problem has been solved six times: Figs.3a-3b-3c are referred to linear forces along the axes in Eq.(20), while Figs.3d-3e-3f concern torques.

	MI	μ	ρ_x	ρ_y	ρ_z
(a)	6.92e-5	9.95e4	154.17	**172.00**	0.55
(b)	1.15e-4	2.74e5	154.17	**172.00**	0.33
(c)	8.02e-6	14.03	25.35	51.78	**94.95**
(d)	0.03	1.41e6	**0.27**	8.93e-5	0.03
(e)	4.14e-10	1.13e15	6.61	**1.11e8**	3.29
(f)	181.13	5.50	0.16	0.12	**0.28**

Table 2: Numerical results of reported cases.

(a) All the legs reach their own kinematic singularities. The ellipsoid converges to an ellipse almost in the X-Y plane: it means that the structure is much more able to reject forces along those directions with respect to vertical.
(b) The current SILVER2 configuration is very similar to case (a) since it prevents movements in the X-Y plane.
(c) The pose of the robot permits to maximize the length of the ellipsoid along the Z-axis. Consequently, the hexapod can sustain larger forces on the vertical direction than on others.
(d) SILVER2 assumes this configuration to prevent rotations around the X-axis; this is the reason why the torque ellipsoid is maximised along the X direction.

(e) The current configuration can be explained as the case (d), but along the Y-axis. The ellipse collapses on a straight line, consequently the parallel structure is near to a singular configuration.
(f) Rotations around the vertical axis are limited, but admitted. The current legs configuration limits the twist of the body around Z.

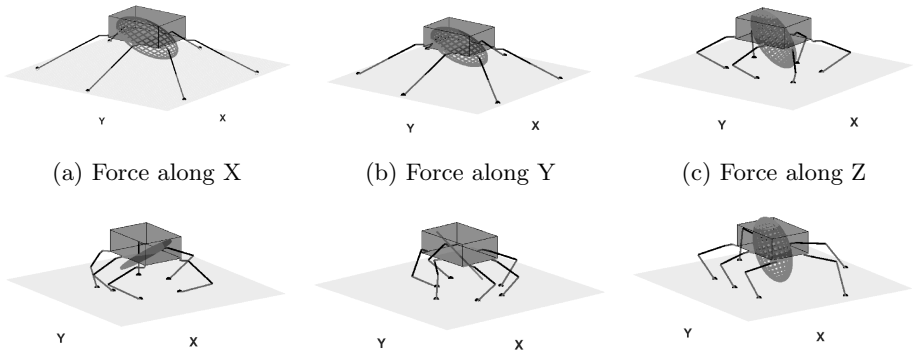

(a) Force along X (b) Force along Y (c) Force along Z

(d) Torque around X (e) Torque around Y (f) Torque around Z

Fig. 3: Optimal solutions to the SILVER2 Statics. The ellipsoids have been normalised with respect to the longest semi-axis.

In a previous work [15], a soft continuum arm was installed on the hexapod. Among other tests, the amount of force exerted by the action of the legs alone was measured, being 44 N on the vertical direction. By simulating the same experimental conditions, the ellipsoid semi-axis along the Z direction is 47.36, which increases to 50 following the proposed optimization procedure. Even if this experimental condition was already close to the maximum value, in other directions (see Fig.3) the stance will be not trivial and may significantly diverge from initial guesses.

4 Discussion

The hexapod robot SILVER2 has been modeled as a Stewart platform. The main difference among the two robots consists in the fact that the serial actuators of the parallel manipulator have a fixed position on the ground, whereas SILVER2 is capable of independently positioning its feet within the work-space of its 3 DOFs segmented legs. This difference leads to two major consequences, on one hand, when SILVER2 stands with all its feet on the ground it presents a wider work-space with respect to its counterpart. On the other hand, the feet of SILVER2 may slip on the seabed, with the consequent lost of the static configuration. In addition to that, when operating SILVER2 underwater, external disturbances such as currents may occur. In this work feet slipping and currents have been neglected. The former assumption is justified by the possibility of developing high friction feet, for example through the use of micro-spines [27], or operating on high friction surfaces. The latter assumption is justified by the possibility

of operating SILVER2 in low current environment, as commonly done for other underwater vehicles or by exploiting poses which result in low hydrodynamic disturbances (e.g. low stance).

In particular in this work, force/moment ellipsoids have been introduced as a tool to characterize the statics of the hexapod. They are helpful to understand how much force/moment the robot can resist along/around a certain direction with respect to others: the longer the distance between the center of the ellipsoid and its surface along a given direction, the greater will be the maximum force/moment that the robot can resist along/around it.

This way of thinking may be very helpful in case of manipulation tasks. It may happen that the robot is not able to resist enough force along the required direction. Consequently, moving the legs in order to obtain the force ellipsoid with the largest projection towards the desired direction may solve the problem. The same reasoning could be done in the case of torque ellipsoids.

Several optimal solutions have been reported in Fig.3. Once the pose of the body is chosen, the best configuration of the legs is computed via an optimization procedure. We have reported the results relative to forces and torques along/around the three axes of the world frame, however any arbitrary direction can be chosen by the user according to the task to fulfill.

The reason why the optimizer gives the reported solution as output can be better explained via the manipulability ellipsoid. Indeed, since manipulability and force ellipsoid are inversely proportional, a higher manipulability along the shortest force ellipsoid's axes is observed; it means that along those axes, the robot is able to move much more easily. For instance, Fig.3a represents the configuration which optimizes the forces exerted along the X-axis; in this case, the robot is much more able to move on the Z-axis direction instead of the X- and Y-axes because of the straight legs. A similar reasoning can be done in the case of rotations and moments as shown in Fig.3d. The configuration prevents rotations with respect to the X-axis, but allows movements around Y- and Z-axes.

The mathematical tool proposed in this work may be helpful to optimize the static configuration of legged robots, while interacting with the external environment. The pose of the body could be chosen accordingly to the task to be completed, and further developments could involve the increase of the degrees of freedom during the optimization process (e.g. the position of the body in the case of required rotation, or vice versa). Moreover, the presented optimization procedure can be generalized to include, along with static loads, dynamic ones. Further developments may include the realization of a physical simulator and an actual experimental setup, to support simulation results and validate the model.

References

1. Francisco, R., Valero, F., Llopis-Albert, C., 2019. A review of mobile robots: Concepts, methods, theoretical framework, and applications. *International Journal of Advanced Robotic Systems*, 16(2).
2. Ortigoza, R.S., et al., 2012. Wheeled mobile robots: a review. *IEEE Latin America Transactions*, 10(6).

3. Hassanalian, M., Abdessattar, A., 2017. Classifications, applications, and design challenges of drones: A review. *Progress in Aerospace Sciences*, 91, 99-131.
4. Bogue, R.,2015. Underwater robots: a review of technologies and applications. *Industrial Robot*, 42(3), 186-191.
5. Calisti, M., Picardi, G., Laschi, C., 2017. Fundamentals of soft robot locomotion. *Journal of The Royal Society Interface*, 14(130).
6. Silva, M.F., Machado, T., 2012. A literature review on the optimization of legged robots. *Journal of Vibration and Control*, 18(12), 1753-1767.
7. Khatib, O., 1999. Mobile manipulation: The robotic assistant. *Robotics and Autonomous Systems*, 26(2), 175-183.
8. Bayle, B., Fourquet, J-Y., Renaud, M., 2003. Manipulability of wheeled mobile manipulators: Application to motion generation. *The International Journal of Robotics Research*, 22(7), 565-581.
9. Rehman, B.U., et al., 2016. Towards a multi-legged mobile manipulator. *ICRA*.
10. Galvez, J.A., Estremera, J., Gonzalez De Santos., P., 2003. A new legged-robot configuration for research in force distribution. *Mechatronics*, 13(8), 907-932.
11. Ding, X., Yang, F., 2014. Study on hexapod robot manipulation using legs. *Robotica*, 34, 468-481.
12. Katz, D., et al., 2006. The umass mobile manipulator uman: An experimental platform for autonomous mobile manipulation.
13. Youakim, D., et al., 2017. Moveit!: Autonomous underwater free-floating manipulation. *IEEE Robotics Automation Magazine*, 24(3), 41-51.
14. Conti, R., et al., 2017. A free floating manipulation strategy for Autonomous Underwater Vehicles. *Robotics and Autonomous Systems*, 87: 133-146.
15. Liu, J., et al., 2020. Underwater Mobile Manipulation: A Soft Arm on a Benthic Legged Robot. *IEEE Robotics and Automation Magazine*, 27(4), 12-26.
16. Dash, A.K., Chen, I.M., Yeo, S.H., Yang, G., 2005. Task-oriented configuration design for reconfigurable parallel manipulator systems. *International Journal of Computer Integrated Manufacturing*, 18(7), 615-634.
17. Camacho-Arreguin, J., Wang, M., Dong, X., Axinte, D., 2020. A novel class of reconfigurable parallel kinematic manipulators: Concepts and Fourier-based singularity analysis. *Mechanism and Machine Theory*, 153.
18. Russo, M., Dong, X., 2020. A calibration procedure for reconfigurable Gough-Stewart manipulators. *Mechanism and Machine Theory*, 152.
19. Picardi, G., Laschi, C., Calisti, C. 2018. Model-based open loop control of a multi-gait legged underwater robot. *Mechatronics*, 55, 162–170.
20. Stewart, D., 1965. A platform with six degrees of freedom. *Proceedings of the Institution of Mechanical Engineers*, 180(1), 371-386.
21. Mendes Lopes, A., Gomes de Almeida, F., 2003. Manipulability Optimization of a Parallel Structure Robotic Manipulator. *Multibody System Dynamics*, 9(1), 1-23.
22. Gewald, D., Dynamics and control of hexapod systems.
23. Ropponen, T., Arai, T., 1995. Accuracy analysis of a modified Stewart platform manipulator. *1995 IEEE ICRA*.
24. Picardi, G., et al., 2020. Bioinspired underwater legged robot for seabed exploration with low environmental disturbance. *Science Robotics*, 5(42).
25. Lynch, K.M., Park, F.C., 2017. Modern Robotics: Mechanics, Planning, and Control. *Cambridge University Press*, 1st edition.
26. Yoshikawa, T., 1985. Manipulability of Robotic Mechanisms. *The International Journal of Robotic Research*, 4(3).
27. Wang, S., Jiang, H., Cutkosky., M.R., 2016. A palm for a rock climbing robot based on dense arrays of micro-spines. *2016 IEEE IROS*.